Heat transfer analysis of silver-water nanofluid flow over stretching cylinder subjected to multiple convective conditions over stretching sheet and stretching cylinder*

[a]

Abstract

The study investigate the MHD flow over a stretching cylinder containing silver-water nanofluid in the presence of a magnetic field under multiple convective boundary conditions over stretching sheet and stretching cylinder. A system of PDEs is reduced to a solvable system of ODEs by applying a suitable similarity transformation. We employ the Runga Kutta method to solve the flow, heat, and mass transfer equations along with boundary conditions. The plots illustrate the effect of different dimensionless parameters on velocity, temperature, and concentration profiles. Two-dimensional graphs and tables of rate of heat transfer and skin friction estimates are provided. Significant role of Biot number on temperature and concentration profile was observed. Nusselt number increases with Bi and Pr. The skin friction is enhanced with M but decrease with λ

Keywords: MHD, Mixed convection, nanofluid, Numerical analysis

2010 MSC: 00-01, 99-00

1. Introduction

The addition of nanoparticles to a base fluid, the elasticity of surfaces, the application of a magnetic flux, the addition of artificial surface roughness, the attachment of fins, and the insertion of barriers are mechanisms for enhancing passive heat transfer. Over the past few decades, scientists have worked very hard to create novel nanofluids that perform better. A hybrid nanofluid is a nanofluid that contains two or more nanoparticles. Numerous studies have demonstrated that hybrid nanofluids are superior to single nanofluids. Compared to hybrid nanoparticles, single nanoparticles had a less impact on temperature dispersion. Choi and Eastman [1] first identified the unique heat transmission and cooling properties of nanofluid. They found that the physical and chemical characteristics of the standard fluid and nanofluid are different, and proposed nanofluid as a suspension of nanoparticles (1-100 nm in size) in the base fluid. Bagh et al. [2] investigated the 3D convective heat transfer features of a magneto hydrodynamic nanofluid flow that comprised oxytactic motile microorganisms and nanoparticles and flowed through a rotating cone. The impact of thermal energy, velocity profiles, and concentration slip on an MHD flow of a nanofluid constrained by Sohaib et al. [3] over the stretching surface. Williamson nanofluid flow with the effects of thermal radiation and thermo-diffusion

*Fully documented templates are available in the elsarticle package on CTAN.

*

[a,*])

through a porous stretching/shrinking sheet was examined by Bhatti and Rashidi [4]. Buongiorno [5] created a mathematical model that illustrates the thermophoresis and Brownian motion of nanoparticles. Many researchers have been concentrating on the creation and utilisation of nanofluids in various areas, especially in the case of stretching sheets [6, 7, 8, 9] and cylinders [10, 11, 12]. Ibrahim et al. [13] examined the MHD Williamson liquid over a stretching cylinder with the importance of activation energy. Gouran et al. [14] examined the effects of thermal radiation on nanofluid flow between two circular cylinders under the influence of a magnetic field. In contrast to the conventional Fourier's equation of heat conduction, Dogonchi and Ganji [15] investigated an unstable squeezing MHD nanofluid flow and heat transfer between two parallel plates in the presence of thermal radiation impact. Theoretical analysis was done by Abdelhafez et al. [16] on the Magnetohydrodynamic (MHD) flow over a nanofluid through a porous medium induced by a solar energy stretching sheet. Arifin et al.[17] examined the magnetohydrodynamic, suctional, and Joule heating effects on the horizontally stretched/shrinking layer as well as the dynamics flow and thermal expansion of the hybrid Cu Al2O3/water nanofluid. The flow of third-grade nanofluid through a stretched cylinder was discussed by Shafiq et al. [18]. The bioconvection analysis for nanofluid flow in a square cavity was carried out by Mansour et al. [19]. In a porous channel with such a mass flow characteristic, Sharmaet al. [20] investigated the effects of buoyancy and flow rate over Sisko nanoparticles across a vertical stretched surface. The magnetohydrodynamic Ag/water nanofluid is examined in a two-dimensional continuous flow over a stretching cylinder or flat sheet. The set of higher-order partial equations was transmuted to lower-order differential equations and numerically solved under physically realistic boundary conditions. This flow regime can be found in technological mechanisms for mechanical means such as shrink packing, shrinking film, shrinkage wrapping, and thermal procedure. The fluctuating trends of physical outcomes are particularly noticeable for velocity, temperature functions, and the results are graphed with other physical factors such as stratification, concentration, and buoyancy factors. In this scenario, the current description goes ahead in pursuit of the responses to the following quarries:

2. Physical Pattern and Interpretation

The magneto hydrodynamic Ag/water nanofluid is examined in a two-dimensional continuous flow over a stretching cylinder or flat sheet sketched in Fig.1. This section shows a mathematical model for analyzing heat and mass transfer in a two-dimensional nanofluid flow towards a cylinder with radius R with free stream velocity U_∞ has been consider. The impacts of convective boundary conditions are included in this paper to broaden the scope of the research. Let free stream velocity $u_w = \frac{ax}{l}$ flow over the cylinder, where a is a positive constant. The coordination system takes into consideration the x-axis along the cylinder's surface and the r along the axial direction. The surface temperature is the result of convective heating from a hot fluid, expressed with T and h_f is the thermal efficiency. The thermo-physical properties of nanoparticles are shown in Table 1. The Tiwari and Das model have been taken into consideration. The

governing equations are given in light of the above assumptions:

$$\frac{\partial(ru)}{\partial x}+\frac{\partial(rv)}{\partial r}=0 \tag{1}$$

$$u\frac{\partial u}{\partial x}+v\frac{\partial u}{\partial r}=\frac{\mu_{hnf}}{\rho_{hnf}}\left(\frac{\partial^2 u}{\partial r^2}+\frac{1}{r}\frac{\partial u}{\partial r}\right)-\frac{\sigma B_0^2}{\rho_{hnf}}u+\left[\frac{(\rho\beta)_{hnf}}{\rho_{hnf}}g(T-T_\infty)\right] \tag{2}$$

$$(\rho C_p)_{hnf}\left(u\frac{\partial T}{\partial x}+v\frac{\partial T}{\partial r}\right)=\kappa_{hnf}\left(\frac{\partial^2 T}{\partial r^2}+\frac{1}{r}\frac{\partial T}{\partial r}\right) \tag{3}$$

$$u\frac{\partial C}{\partial x}+v\frac{\partial C}{\partial r}=D_m\left(\frac{\partial^2 C}{\partial r^2}+\frac{1}{r}\frac{\partial C}{\partial r}\right)+\frac{D_m k_t}{T_m}\left(\frac{\partial^2 T}{\partial r^2}+\frac{1}{r}\frac{\partial T}{\partial r}\right) \tag{4}$$

According to the problem's geometry, the boundary conditions can be divided into the preceeding classes:

$$\left.\begin{aligned}&(a)\quad u=U_w=0,\quad v=0,\quad \kappa_{nf}\frac{\partial T}{\partial r}=-h_{nf}\{T_w-T\},\quad D_n\frac{\partial C}{\partial r}=-h_f\{C_w-C\}at\quad r=R\\&(b)\quad u\to u_w=\frac{ax}{l},\quad T\to T_\infty,\quad C\to C_\infty,\quad at\quad r\to\infty\end{aligned}\right\} \tag{5}$$

Where u and v are the velocity components along x and r directions. And $\{\kappa/(\rho C_p)_f\}$, the thermal conductivity of fluid is κ and specific heat is C_p. The fluid temperature is (T), and (B_0) is the magnetic field parameter, dynamic viscosity (μ) and the density of the based fluid is (ρ). With the exception of density changes that create a thermal buoyancy force retains consistent characteristics.

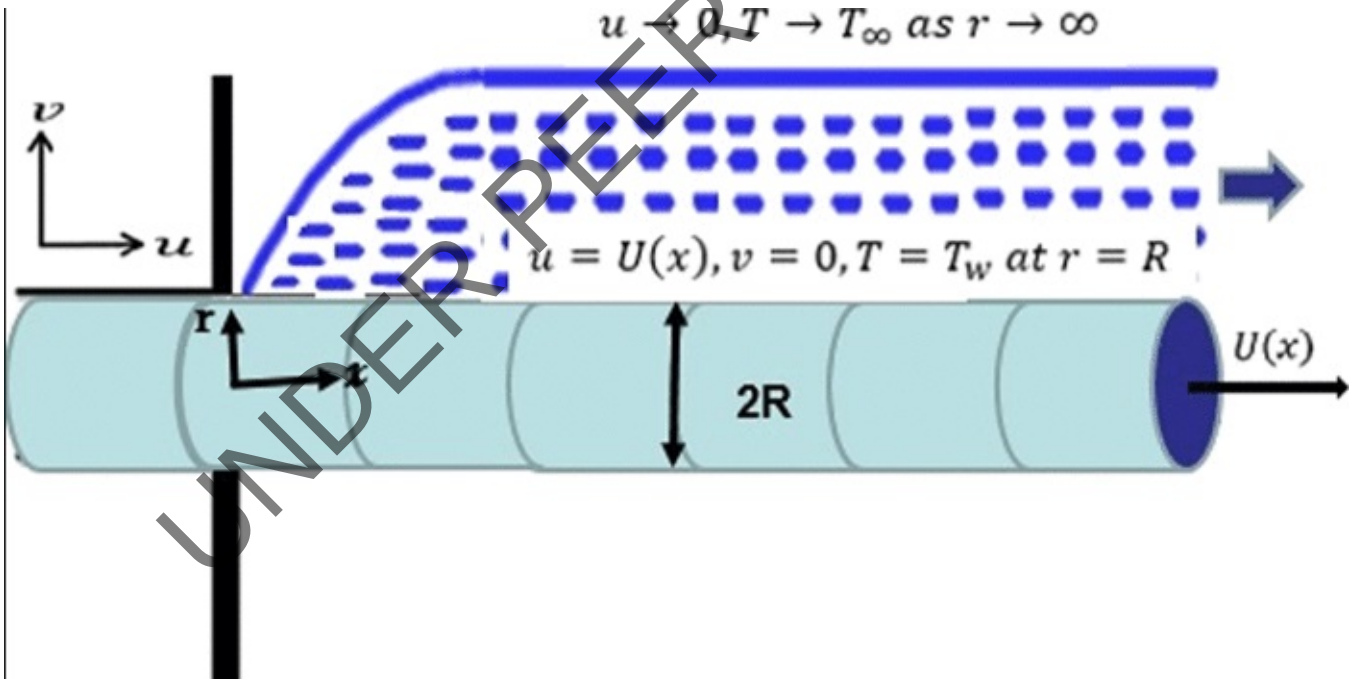

Figure 1: Physical flow diagram

Table 1: The physical Properties [21, 22].

Physical properties	$\rho(kg.m^{-3})$	$C_p(J/kg \cdot K)$	$\kappa(W/m \cdot K)$	$\sigma \times 10^5\ k^{-1}$
H_2O	0997.1	4179.0	00.613	2.1 $\times 10^{-4}$
Ag	10500	235.00	429.00	1.89 $\times 10^{-5}$

Table 2: Thermophysical properties of water and nanofluid [23, 24]

Properties	Nanofluid
Density (ρ)	$\frac{\rho_{nf}}{\rho_f} = (1-\phi) + \frac{\rho_s}{\rho_f}\phi$
Viscosity (μ)	$\mu_{n_f} = \frac{\mu_f}{(1-\phi)^{2.5}}$
Heat capacity (ρC_p)	$\frac{(\rho C_p)_{nf}}{(\rho C_p)_f} = (1-\phi) + \frac{(\rho C_p)_s}{(\rho C_p)_f}\phi$
Electrical conductivity (σ)	$\frac{\sigma_{nf}}{\sigma_f} = 1 + \frac{3(\sigma-1)\phi}{(\sigma+2)-(\sigma-1)\phi}$

Table 2 shows that the subscriptsf_s and n_f stand for fluid, solid nanoparticles of Ag, and nanofluid, respectively. By introducing the non-dimensional variables below, the elaborated problem's complexity is simplified.:

$$\left.\begin{aligned} \Phi(x,r) = R\sqrt{u_w \nu_f x}F(\xi),\ \xi = \frac{r^2-R^2}{2R}\left(\frac{u_w}{\nu_f x}\right)^{\frac{1}{2}},\ u_w = \frac{ax}{l}\ \theta(\xi) = \frac{T-T_\infty}{T_w-T_\infty}, \\ ru = \frac{\partial \Phi}{\partial r}, \psi(\xi) = \frac{C-C_\infty}{C_w-C_\infty},\ rv = -\frac{\partial \Phi}{\partial x}, \end{aligned}\right\} \tag{6}$$

Here the stream functions Φ and ξ are dimensionless. In order to satisfy equation 1, the Φ stream function is typically defined. Then, using the similarity vectors (6) mentioned above, the non linear partial differential equations (2-4) are transformed as follows:

$$(2\xi\Gamma+1)F^{'''} + 2\Gamma F^{''} + \frac{B_3}{B_1}\lambda\theta + \frac{B_2}{B_1}\left[1 + FF^{''} - \left(F^{'}\right)^2\right] - \frac{MB_3}{B_1}F^{'} = 0 \tag{7}$$

$$\left[(2\xi\Gamma+1)\theta^{''} + 2\Gamma\theta^{'}\right] + \frac{B_5}{B_4}P_r\left[F\theta^{'}\right] = 0 \tag{8}$$

$$(1+2\xi\Gamma)\psi^{''} + (LeF + 2\Gamma)\psi^{'} + Sr\left[(1+2\xi\Gamma)\theta^{''} + 2\Gamma\theta^{'}\right] = 0 \tag{9}$$

$$\tag{10}$$

Moreover, the modified boundary conditions are as follows;

$$\left.\begin{aligned} F(\xi) = 0,\ F^{'}(\xi) = 0,\ \theta'(\xi) = -Bi\{1-\theta(0)\},\ \psi'(\xi) = -Bi_2\{1-\psi(0)\},\ at\ \xi = 0 \\ F^{'}(\xi) \to 1,\ \theta(\xi) \to 0,\ \psi(\xi) \to 0, at\ \xi \to \infty \end{aligned}\right\} \tag{11}$$

and the transformed boundary conditions are described as; The thermos-physical factors are explained such as; [25]

$$B_1 = (1-\phi)^{2.5}, \quad B_2 = \{(1-\phi) + \frac{\rho_s}{\rho_f}\phi\} \qquad B_3 = \frac{\sigma_{nf}}{\sigma_f} = 1 + \frac{3(\sigma-1)\phi}{(\sigma+2)-(\sigma-1)\phi}$$

$$B_5 = \frac{k_s + (s_f-1)k_{bf} - (s_f-1)(k_f-k_s)\phi}{k_s + (s_f-1)k_{bf} + (k_f-k_s)\phi}$$

$$B_4 = \frac{(\rho C_p)_{nf}}{(\rho C_p)_f} = (1-\phi) + \frac{(\rho C_p)_s}{(\rho C_p)_f}\phi$$

3. Physical Quantities

The various involving parameters in equations (08) to (13) are also described, as are the numerous participating parameters are Prandtl number (P_r), Magnetic parameter (M), traditional Lewis number (L_e), Biot number (B_i), Lewis number (L_b), mixed convection parameter (λ), Grashof number (G_r), Reynolds number, (S_r) Soret number, thermally stratified variable (θ_t) and the curvature parameter (Γ).

$$\left.\begin{aligned} M = \frac{\sigma_f {B^2}_0 l}{\rho_f a},\ Sr = \frac{k_t(T_w - T_\infty)}{T_m(C_w - C_\infty)}, \\ Le = \frac{\mu_f}{\rho_f D_m}, \lambda = \frac{G_r}{R_E},\ G_r = \frac{\beta_f g(T_w - T_\infty l^3)}{\nu_f^2},\ R_e = \frac{U - \omega l}{\nu_f},\ Pr = \frac{\mu_f}{\rho_f \alpha_f} \\ \Gamma = \frac{1}{R}\sqrt{\frac{\mu_f l}{\rho_f a}},\ Bi = \frac{Rh_{nf}}{(\kappa_{nf})r}\sqrt{\frac{l\nu_f}{a}},\ \alpha_f = \frac{\kappa_f}{(\rho c)_f} \end{aligned}\right\}$$

4. Engineering Quantities

The requisite aspects of engineering interest skin friction coefficient C_{fx}, local Nusselt number Nu_x, local Sherwood number Sh_x, and the bioconvective number B_1 are the practical interest quantities as follows:

$$C_{fx} = \frac{2\mu_{nf}}{\rho U_\infty^2}\left(\frac{\partial u}{\partial r}\right)_{r=R}, \quad Nu_x = \frac{x\kappa_{nf}}{\kappa(T_w - T_\infty)}\left(\frac{\partial T}{\partial r}\right)_{r=R} \tag{12}$$

In view of the above similarity transformation functions (8), can be calculated as:

$$C_{fx} = \sqrt{Re_x}C_f = 2B_1\frac{d^2F(0)}{d\zeta^2}, \quad \frac{Nu_x}{\sqrt{Re_x}} = -1B_5\{\theta'(0)\}, \quad \frac{Sh_x}{\sqrt{Re_x}} = -\phi'(0),$$

where $Re_x = xu_w/\nu_f$ is the local Reynold's number.

5. Execution of Methodology

The system of ODE's is numerically solved by the RK technique. In which estimates the mathematical solutions numerically using an adaptive Runge-Kutta method (for solutions) in Matlab and for shooting we implemented the Newton-Raphson method [**?**]. We do this by first assuming:

$f_1 = \Pi_1,\ \ f_1' = \Pi_2,\ \ f_1'' = \Pi_3$

$\theta = \Pi_4,\ \ \theta' = \Pi_5, \Phi = \Pi_6,\ \ \Phi' = \Pi_7,$

$\zeta = \Pi_8, \ \zeta' = \Pi_9$

$\Pi_1' = \Pi_2$

$\Pi_2' = \Pi_3$

$\Pi_3' = \frac{-1}{(1+2\Gamma\xi)}[2\Gamma\Pi_3 + \frac{B2}{B1}(1 + \Pi_1\Pi_3 - \Pi_2^2) + \frac{B3}{B1}\lambda\Pi_4 - \frac{MB_3}{B1}\Pi_2]$

$\Pi_4' = \Pi_5$

$\Pi_5' = \frac{1}{(B_4(1+2\Gamma\xi))}[2B_4\Gamma\Pi_5 + B_5(P_r)(\Pi_1\Pi_5)]$

$\Pi_6' = \Pi_7$

$\Pi_7' = \frac{-1}{(1+2\Gamma\xi)}[(2\Gamma + L_e\Pi_1)\Pi_7 + S_r(1 + 2\Gamma\xi)(\Pi_5') + 2\Gamma\Pi_5)]$

with

$\Pi_1(0) = 0, \ \Pi2(0) = 1, \ \Pi_3(0) = \Delta_1, \ \Pi_4(0) = \Delta_2, \ \Pi_5(0) = Bi(1 + \Pi_4(0)), \ \Pi_7(0) = Bi_2(1 + \Pi_6(0))$

$\Pi_7(0) = \Delta_3, \ \Pi_8(0) = 1,$

where $\Delta_1, \ \Delta_2, \ \Delta_3$, are calculated with an appropriate initial guess using the Newton Raphson technique. The numerical technique (Runge Kutta) was validated, and it was found to have an excellent agreement in table3.

Table 3: Comparison of $-\theta'(0)$ for different values of P_r and other parameters are constant

P_r	Gorla and Sidawi [26]	Khan and pop [27]	Hamad [28]	Present result
00.02	00.1691	00.1691	0.16908	0.169087
00.70	00.5349	00.4539	0.45395	0.453912
02.08	00.9114	00.9113	0.91134	0.911357
07.00	01.8905	01.8954	1.89545	1.895405
20.00	03.3539	03.3539	3.35392	3.353929
70.00	06.4622	06.4622	6.46220	6.462364

6. Results and Discussion

Table 4 shows the numerical validation and the comparison of the present study with previous results. The stimulus of various parameters has an impact on momentum profile $F(\xi)$, thermal distribution $\theta(\xi)$, nanoparticle concentration profile $\psi(\xi)$ is investigated for both stretching cylinder and a flat sheet scenario, which is revealed in Figures (2(a-b)-6(a-b)) It is remarked that all graphical analysis is performed for flow confined by stretched cylinder $(\Gamma = 0.5)$ and flow due to flat plate $(\Gamma = 0.0)$. To accomplish this purpose, figures and tables are presented. Figure (2a) revealed magnetic field qualities on the velocity profile. we can see from this diagram that the dimensionless velocity falls as the magnetic parameter increases for both surfaces. The increasing change in F' is comparatively more progressive for flat plate configuration. The Lorentz force is induced by the presence of a transverse magnetic field in an electrically conducting liquid, which slows the fluid' s flow within the boundary layer area. The impact of the mixed convection parameter λ on the velocity profile is shown in Figure (2b). The velocity profile enhanced with λ whereas thermal

layer decreases for both sheet and cylinder surfaces. The increasing change in F' is comparatively more progressive for flat plate configuration. Physically the ratio of inertial to buoyant forces is the mixed convection parameter, an increase in λcorrelates to increased thermal buoyancy forces, which improves velocity profiles. Figure (3a-3b) depicts the relationship between the magnetic parameter with the concentration and temperature distributions for both stretchable cylinder and sheet cases. As the magnetic parameter' s values rise, the thermal boundary layer and concentration layer become thicker. The Lorentz drag, which acts as an opposing force, helps to increase the frictional heating between the fluid layers, which results in the release of energy in the form of heat. As a result, the thermal boundary layer thickens. The Figure (4a) depict the dropping impact of the velocity profile with Prandtl number Pr for both stretching cylinder and a flat sheet scenario. The higher the Pr, the more viscous the fluid, causing the boundary layer to thicken, reducing shear stress and therefore retarding the nano fluid' s flow. Figure (4b), describe the influence of Prandtl number Pr on nanoparticle temperature. Again, results are prepared by stretched cylinder $\Gamma = 0.5$ and flow due to flat plate $\Gamma = 0.0$. The Prandtl number is a non-dimension quantity, defined as the ratio of two quantities momentum and thermal diffusivity. Thermal diffusivity diminishes when Pr rises which further gives a drop-in boundary layer thickness and temperature. The impact of the mixed convection parameter λ on the temperature profile is shown in Figure (5a). The thermal layer decreases for both sheet and cylinder surfaces. Figure (5b) illustrates the observation that the thermal layer and becomes a more noticeable characteristic of fluid layers with rising Biot number Bi both stretchable cylinder and sheet cases. Both profiles enhanced with Bi. Convective heating occurs at the sheet more frequently and intensifies as Bi increases, increasing the temperature. If the variation is greater, the thermal influence can reach the quiescent fluid. In addition, as the fluid temperature rises, the stretched sheet's right-hand side Biot number increases, decreasing its thermal resistance and increasing convectional heat transfer. Figure (6a) illustrates the observation that the concentration profile becomes a more noticeable characteristic of fluid layers with rising Biot number Bi_2 both stretchable cylinder and sheet cases. The profiles enhanced with Bi_2. A decrease in concentration profile can be observed with increased Sr parameter values both stretchable cylinder and sheet cases is shown in Figure (6b). Table (**??**) elucidate the variation of pertinent parameters on heat transfer and drag coefficient. Further a decreasing effects on the skin coefficient with increasing in magnetic field M and λ but remains constant with $P_r, and B_i$. While nusselt number reinforce with increasing in parameters P_r, Biot number B_i and λ where as decreasing function of magnetic field M. Also we compare the stretching sheet with that of the stretching cylinder.

Table 4: The Comparison of Nusselt number (Nu_x) and skin friction coefficient (Cf_x) for Stretching Sheet and Stretching cylinder with different values of M, λ, Pr, Bi while other parameters remain fixed.

M	λ	Pr	Bi	Stretching Sheet $Nu_x Re_x^{-1/2}$	Stretching Sheet $\frac{1}{2}C_f x_x^{-1/2}$	Stretching Cylinder $Nu_x Re_x^{-1/2}$	Stretching Cylinder $\frac{1}{2}C_f x_x^{-1/2}$
0.1	0.1	0.5	0.1	0.209526	0.656857	0.204496	0.822342
0.3	-	-	-	0.206775	0.748592	0.203875	0.885590
0.5	-	-	-	0.203778	0.862956	0.201078	0.993657
0.3	0.2	0.5	0.1	0.205185	0.773839	0.202783	0.908940
-	0.4	-	-	0.205556	0.761340	0.203059	0.896035
-	0.6	-	-	0.206154	0.750920	0.203754	0.885141
0.3	0.2	0.1	0.1	0.302991	-1.057740	0.252993	0.787404
-	-	0.3	-	0.377056	0.877402	0.287054	0.787404
-	-	0.5	-	0.390285	0.877403	0.310283	0.784041
-	-	-	0.1	0.237241	0.877403	0.207278	0.677395
-	-	-	0.2	0.373043	0.577409	0.273065	0.677409
-	-	-	0.5	0.572047	0.577402	0.044202	0.677410

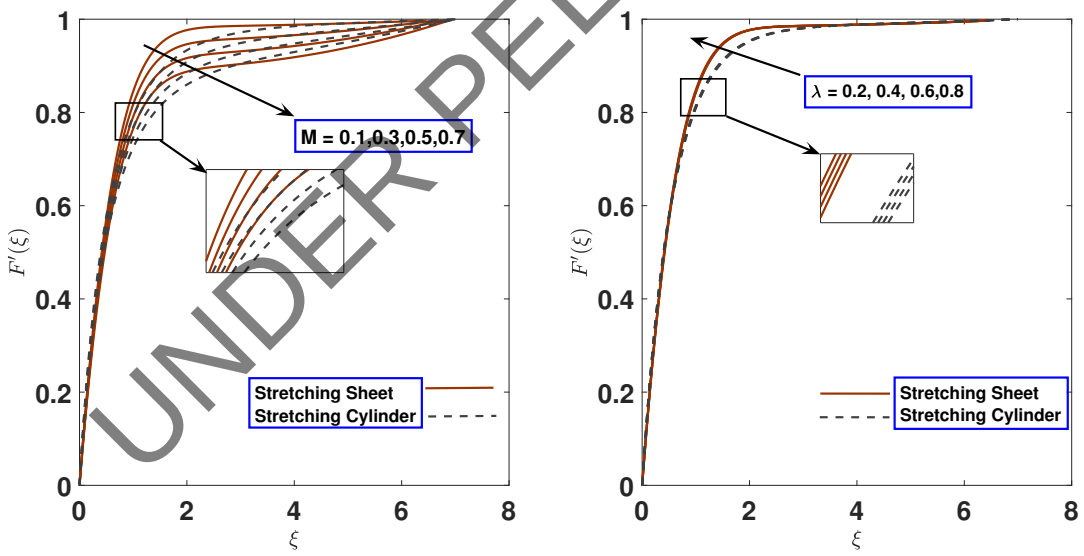

Figure 2: (a-b) Fluctuation of Velocity profile along with variation of M and λ.

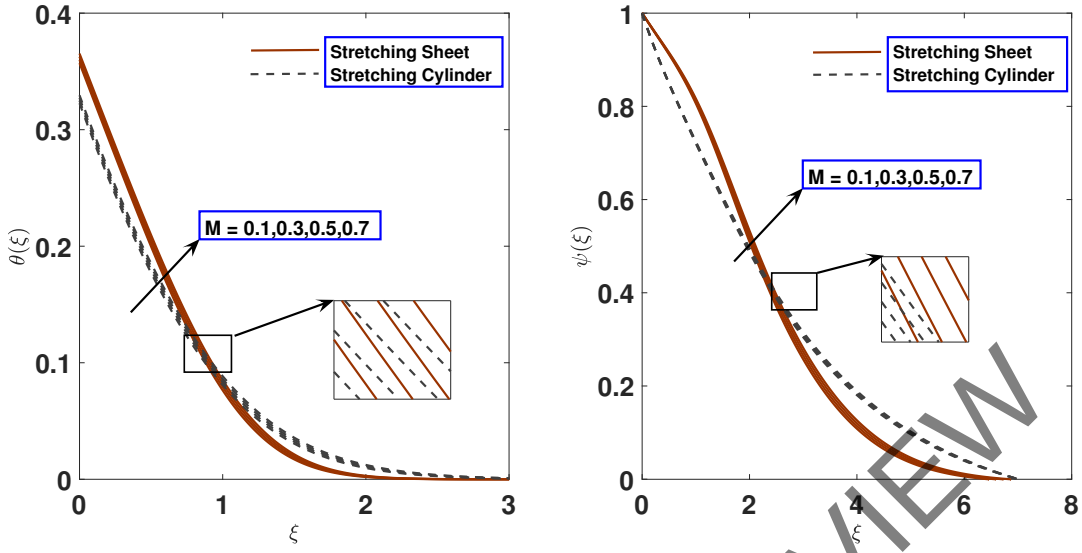

Figure 3: (a-b) Fluctuation of Temperature profiles and concentration profile along with M

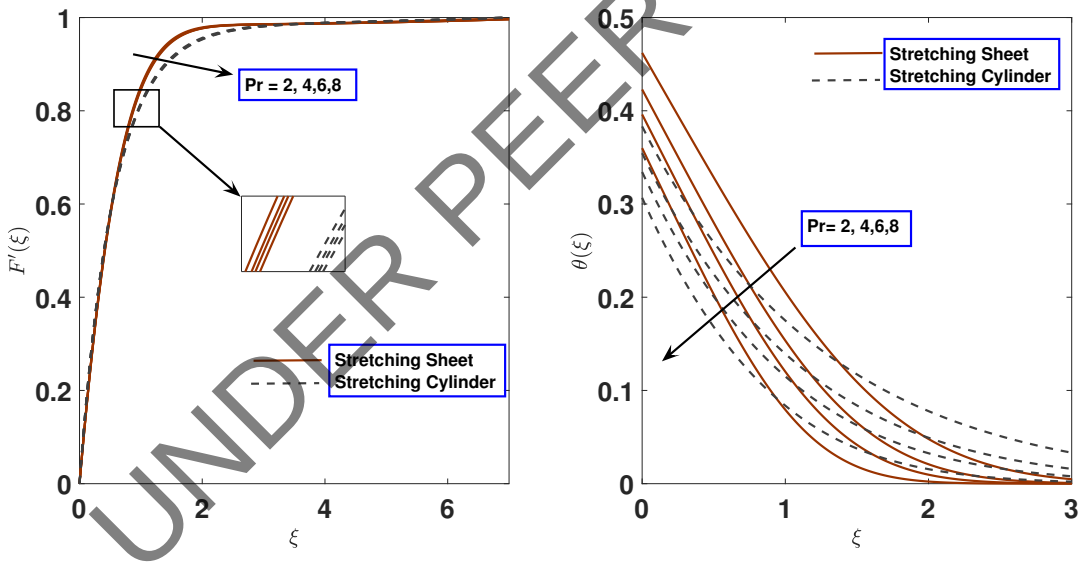

Figure 4: (a-b) Variation in velocity and temperature profile against η for different values of Pr

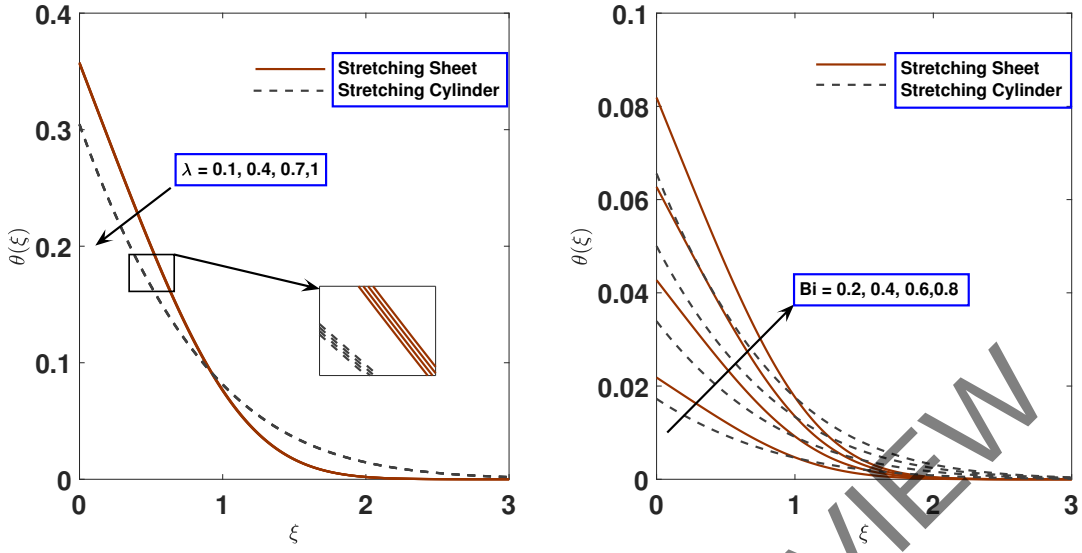

Figure 5: (a-b) Variation in velocity profile against η for different values of R_d and λ_θ

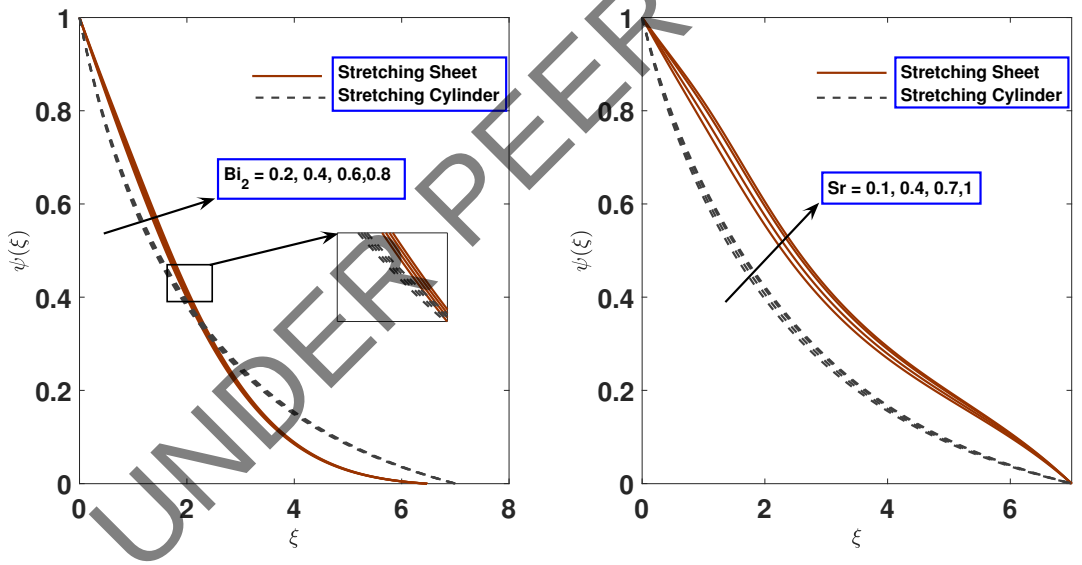

Figure 6: (a-b) Fluctuation of concentration profiles along with different values of Bi_2 and Sr

7. Concluding Remarks

In this paper, presents the stretching cylinder and flat sheet along with the multiple convective boundaries condition have been analyzed. Furthermore, the Prandtl number, velocity, and temperature for both stretching cylinder and flate sheet based ag/water nanofluids are provided and compared in this work. The impact of the influential parameters on velocities, skin friction, temperature, Nusselt number, and concentration has been conceived. The following section

summarizes the significant results relating to the variable nature of physical quantities as influenced by the governing parameters:

- Thinning of concentration field relates to increasing values of thermal stratification parameter S_r and with the inclination of values the heat transfer rate accelerates.
- When a stretching cylinder is compared to a flat sheet, the velocity is noticeably greater.
- The nanofluid velocity improved with velocity ratio parameter while magnetic constant reduce the velocity.
- The thickness of thermal boundary layers and heat transfer rates increased due to increase in magnetic field parameters and Biot number.
- Nusselt number reinforce with increasing in parameters P_r, Biot number B_i and λ where as decreasing function of magnetic field M.
- it is observed that skin friction has greater value in case of stretching cylinder that stretching sheet whereas opposite behaviour of Nusselt number.

References

References

[1] S. U. Choi, J. A. Eastman, Enhancing thermal conductivity of fluids with nanoparticles, Tech. rep., Argonne National Lab.(ANL), Argonne, IL (United States) (1995).

[2] L. Ali, X. Liu, B. Ali, S. Mujeed, S. Abdal, Finite element simulation of multi-slip effects on unsteady mhd bioconvective micropolar nanofluid flow over a sheet with solutal and thermal convective boundary conditions, Coatings 9 (12) (2019) 842.

[3] S. Abdal, B. Ali, S. Younas, L. Ali, A. Mariam, Thermo-diffusion and multislip effects on mhd mixed convection unsteady flow of micropolar nanofluid over a shrinking/stretching sheet with radiation in the presence of heat source, Symmetry 12 (1) (2019) 49.

[4] M. M. Bhatti, M. M. Rashidi, Effects of thermo-diffusion and thermal radiation on williamson nanofluid over a porous shrinking/stretching sheet, Journal of Molecular Liquids 221 (2016) 567–573.

[5] J. Buongiorno, Convective transport in nanofluids (2006).

[6] M. Bilal, M. Sagheer, S. Hussain, Three dimensional mhd upper-convected maxwell nanofluid flow with nonlinear radiative heat flux, Alexandria engineering journal 57 (3) (2018) 1917–1925.

[7] M. Sagheer, M. Bilal, S. Hussain, R. Ahmed, Thermally radiative rotating magneto-nanofluid flow over an exponential sheet with heat generation and viscous dissipation: A comparative study, Communications in Theoretical Physics 69 (3) (2018) 317.

[8] A. K. Pandey, M. Kumar, Natural convection and thermal radiation influence on nanofluid flow over a stretching cylinder in a porous medium with viscous dissipation, Alexandria Engineering Journal 56 (1) (2017) 55–62.

[9] M. Ramzan, M. Bilal, Three-dimensional flow of an elastico-viscous nanofluid with chemical reaction and magnetic field effects, Journal of Molecular Liquids 215 (2016) 212–220.

[10] M. Malik, T. Salahuddin, A. Hussain, S. Bilal, M. Awais, Homogeneous-heterogeneous reactions in williamson fluid model over a stretching cylinder by using keller box method, AIP Advances 5 (10) (2015) 107227.

[11] M. Ramzan, M. Bilal, J. D. Chung, Radiative flow of powell-eyring magneto-nanofluid over a stretching cylinder with chemical reaction and double stratification near a stagnation point, PloS one 12 (1) (2017) e0170790.

[12] M. Sheikholeslami, M. Mustafa, D. Ganji, Nanofluid flow and heat transfer over a stretching porous cylinder considering thermal radiation, Iranian Journal of Science and Technology (Sciences) 39 (31) (2015) 433–440.

[13] W. Ibrahim, M. Negera, The investigation of mhd williamson nanofluid over stretching cylinder with the effect of activation energy, Advances in Mathematical Physics 2020 (2020).

[14] S. Gouran, S. Mohsenian, S. Ghasemi, Theoretical analysis on mhd nanofluid flow between two concentric cylinders using efficient computational techniques, Alexandria Engineering Journal 61 (4) (2022) 3237–3248.

[15] A. Dogonchi, D. Ganji, Impact of cattaneo–christov heat flux on mhd nanofluid flow and heat transfer between parallel plates considering thermal radiation effect, Journal of the Taiwan Institute of Chemical Engineers 80 (2017) 52–63.

[16] M. Abdelhafez, A. Abd-Alla, S. Abo-Dahab, Mhd convective non-darcy flow of a nanofluid through a porous stretching sheet with thermal buoyancy and chemical reaction, Waves in Random and Complex Media (2022) 1–18.

[17] N. S. Khashi'ie, N. M. Arifin, R. Nazar, E. H. Hafidzuddin, N. Wahi, I. Pop, Magnetohydrodynamics (mhd) axisymmetric flow and heat transfer of a hybrid nanofluid past a radially permeable stretching/shrinking sheet with joule heating, Chinese Journal of Physics 64 (2020) 251–263.

[18] A. Shafiq, I. Khan, G. Rasool, A. H. Seikh, E.-S. M. Sherif, Significance of double stratification in stagnation point flow of third-grade fluid towards a radiative stretching cylinder, Mathematics 7 (11) (2019) 1103.

[19] M. A. Mansour, A. M. Rashad, B. Mallikarjuna, A. K. Hussein, M. Aichouni, L. Kolsi, Mhd mixed bioconvection in a square porous cavity filled by gyrotactic microorganisms, Int J Heat Technol 37 (2) (2019) 433–445.

[20] R. K. Sharma, A. Bisht, et al., Effect of buoyancy and suction on sisko nanofluid over a vertical stretching sheet in a porous medium with mass flux condition, Indian Journal of Pure & Applied Physics (IJPAP) 58 (3) (2020) 178–188.

[21] T. Hayat, S. Nadeem, Heat transfer enhancement with ag–cuo/water hybrid nanofluid, Results in physics 7 (2017) 2317–2324.

[22] M. H. Esfe, S. Saedodin, M. Biglari, H. Rostamian, An experimental study on thermophysical properties and heat transfer characteristics of low volume concentrations of ag-water nanofluid, International Communications in Heat and Mass Transfer 74 (2016) 91–97.

[23] S. Ghadikolaei, M. Yassari, H. Sadeghi, K. Hosseinzadeh, D. Ganji, Investigation on thermophysical properties of tio2–cu/h2o hybrid nanofluid transport dependent on shape factor in mhd stagnation point flow, Powder technology 322 (2017) 428–438.

[24] S. Ghadikolaei, M. Gholinia, M. Hoseini, D. Ganji, Natural convection mhd flow due to mos2–ag nanoparticles suspended in c2h6o2h2o hybrid base fluid with thermal radiation, Journal of the Taiwan Institute of Chemical Engineers 97 (2019) 12–23.

[25] R. K. Tiwari, M. K. Das, Heat transfer augmentation in a two-sided lid-driven differentially heated square cavity utilizing nanofluids, International Journal of heat and Mass transfer 50 (9-10) (2007) 2002–2018.

[26] R. S. Reddy Gorla, I. Sidawi, Free convection on a vertical stretching surface with suction and blowing, Applied Scientific Research 52 (3) (1994) 247–257.

[27] W. Khan, I. Pop, Boundary-layer flow of a nanofluid past a stretching sheet, International journal of heat and mass transfer 53 (11-12) (2010) 2477–2483.

[28] M. Hamad, Analytical solution of natural convection flow of a nanofluid over a linearly stretching sheet in the presence of magnetic field, International communications in heat and mass transfer 38 (4) (2011) 487–492.